

Alma Mater Studiorum Università di Bologna  
Archivio istituzionale della ricerca

Climate control on stacked paleosols in the Pleistocene of the Po Basin (northern Italy)

This is the final peer-reviewed author's accepted manuscript (postprint) of the following publication:

*Published Version:*

Bruno L., Marchi M., Bertolini I., Gottardi G., Amorosi A. (2020). Climate control on stacked paleosols in the Pleistocene of the Po Basin (northern Italy). JOURNAL OF QUATERNARY SCIENCE, 35(4), 559-571 [10.1002/jqs.3199].

*Availability:*

This version is available at: <https://hdl.handle.net/11585/804868> since: 2021-02-23

*Published:*

DOI: <http://doi.org/10.1002/jqs.3199>

*Terms of use:*

Some rights reserved. The terms and conditions for the reuse of this version of the manuscript are specified in the publishing policy. For all terms of use and more information see the publisher's website.

This item was downloaded from IRIS Università di Bologna (<https://cris.unibo.it/>).  
When citing, please refer to the published version.

(Article begins on next page)

# Climate control on stacked paleosols in the Pleistocene of the Po Basin (northern Italy)

LUIGI BRUNO,<sup>1\*</sup> MICHELA MARCHI,<sup>2</sup> ILARIA BERTOLINI,<sup>2</sup> GUIDO GOTTARDI<sup>2</sup> and ALESSANDRO AMOROSI<sup>3</sup>

<sup>1</sup>Department of Chemical and Geological Sciences, University of Modena and Reggio Emilia, Italy

<sup>2</sup>DICAM Department, University of Bologna, Italy

<sup>3</sup>Department of Biological, Geological and Environmental Sciences, University of Bologna, Italy

---

**ABSTRACT:** Paleosols are recurrent features in alluvial successions and provide information about past sedimentary dynamics and climate change. Through sedimentological analysis on six sediment cores, the mud-dominated succession beneath the medieval ‘Two Towers’ of Bologna was investigated down to 100 m depth. A succession of weakly developed paleosols (Inceptisols) was identified. Four paleosols (P1, P2, P3 and PH) were radiocarbon-dated to 40–10 cal ka BP. Organic matter and CaCO<sub>3</sub> determinations indicate low groundwater levels during soil development, which spanned periods < 5 ka. The development and burial of soils, which occurred synchronously in the Bologna region and in other sectors of the Po Plain, are interpreted to reflect climatic and eustatic variations. Climatic oscillations, at the scale of the Bond cycles, controlled soil development and burial during Marine Isotope Stage (MIS) 3 (P1 and P2). Rapid sea-level oscillations probably induced soil development at the MIS 3/2 transition (P3) and favored burial of PH after 10 ka BP. Weakly developed paleosols in alluvial successions can provide clues to millennial-scale climatic and environmental variations. In particular, the paleosol-bearing succession of the Po Plain represents an unprecedented record of environmental changes across the Late Pleistocene (MIS 3 and 2) in the Mediterranean region. Copyright © 2020 John Wiley & Sons, Ltd.

**KEYWORDS:** alluvial succession; climate control; Pleistocene; Po Basin; weakly developed paleosols.

## Introduction

Paleosols are common features of alluvial successions. Due to their remarkable lateral extent and continuity, they represent effective markers for stratigraphic correlation (Kraus, 1999; McCarthy and Plint, 2003). Their degree of maturity and geometric relationships with associated fluvial-channel bodies provide critical information about sedimentary processes and landscape evolution (Kraus and Bown, 1993; Demko *et al.*, 2004). Moreover, paleosol-bearing successions constitute an excellent terrestrial record of past climate changes (Sheldon and Tabor, 2009; Marković *et al.*, 2012; Srivastava *et al.*, 2018).

Pedostratigraphy has been typically developed in outcrop studies (Cleveland *et al.*, 2007; Dubiel and Hasiotis, 2011). More recently, this technique was applied to the core analysis of late Quaternary successions (Choi, 2005; Tsatskin *et al.*, 2015). A suite of closely spaced paleosols was recently identified

within the mud-dominated alluvial succession beneath the town of Bologna (Amorosi *et al.*, 2014). Only reconnaissance work of these paleosols was carried out in these early studies, which emphasized the correlation potential of buried soil horizons and their geometric relations with channel-related facies. The present study aimed to characterize the sedimentology and geochemistry of these paleosols beneath two Medieval masonry towers (Asinelli and Garisenda, locally referred to as 'Two Towers'). Paleosol stratigraphy was used to reconstruct the sedimentary and pedogenic evolution of the area. In this regard, six sediment cores were recovered within an area of 2000 m<sup>2</sup> around the Two Towers. A total of 245 sediment samples were analyzed for grain size, organic matter and CaCO<sub>3</sub> content. The chronological framework was backed up by 14 radio- carbon dates. The relative influence of external controlling factors (e.g. climate and sea-level oscillations) on soil development was explored through the analysis of a vast stratigraphic and chronological dataset, composed of more than 80 radiocarbon-dated paleosols from cores drilled over a wide portion of the Po Plain.

## Geological setting

The town of Bologna is located at the southern margin of the Po Plain, close to the Apennine foothills. The Apennine fold-and-thrust belt developed from the Late Oligocene to the present (Carminati and Doglioni, 2012) and was generated by the subduction of the west-dipping Adriatic lithosphere beneath Europe (Doglioni *et al.*, 1999). Since the early Pleistocene, large parts of the Northern Apennines, including the area south of Bologna, have been involved in a generalized uplift (Argnani *et al.*, 2003). By contrast, the Po Plain has subsided at rates of 1–2 mm a<sup>-1</sup> in the last 1.43 Ma (Carminati and Di Donato, 1999). The Pliocene–Quaternary Po Basin fill, locally exceeding 8 km in thickness, consists of a shallowing-upward sedimentary succession (Ricci Lucchi, 1986). The uppermost strata, dated to the last 0.87 Ma, are mainly composed of alluvial sediments, supplied by the Po River and its tributaries (Muttoni *et al.*, 2003). Close to the Apennine foothills, fluvial-channel gravels are dominant. Mud-prone interfluvial sectors are preserved only between adjacent river outlets (Amorosi *et al.*, 2014). Two main rivers supply sediments to the Bologna area from two closely spaced (~8 km) river outlets (Fig. 1). The Reno River drains a mountain area of ~1055 km<sup>2</sup> and flows for 212 km, west of Bologna, down to the Adriatic Sea. The Savena River, to the east, is a 55-km-long tributary of the Reno River. Its mountain basin is ~170 km<sup>2</sup>. The Apennine foothills south of Bologna are drained by small creeks, <10 km long, with characteristic torrential regime and low transport capacity. These river courses (Meloncello, Ravone and Aposa in Fig. 2A) drain a cumulative area of just 20 km<sup>2</sup> (Figs 1 and 2A). The subsurface geology of the Bologna urban area is strongly influenced by this configuration. Close to the Reno and Savena outlets, fluvial-channel deposits form multistorey gravel bodies, hundreds of meters thick (Fig. 2A – not shown in cross-sections). Distally, they grade into rhythmical alternations of gravels and muds (Fig. 2B). Pollen analysis of a 300-m-long core (P515, Fig. 2B)

showed that gravel–mud alternations result from climate oscillations at the Milankovitch timescale (~100 ka). In particular, fine-grained deposits include pollen diagnostic of warm-temperate (interglacial) climatic conditions, whereas the onset of fluvial-channel gravel bodies marks the transition to a cold climate (glacial) vegetation (Amorosi *et al.*, 2001). The Marine Isotope Stage (MIS) 6/5 transition (i.e. the base of Late Pleistocene deposits) was placed at 53 m core depth, where a marked upward increase in pollen concentration is associated with the transition from shrubby–herbaceous communities with abundant *Pinus* to pollen indicating a major expansion of relatively thermophilous forests, with *Quercus* as the dominant tree. Coarse-grained fluvial deposits are rare beneath the historical centre of Bologna (Fig. 2B). This area has a relief of 20–30 m above the Reno and Savena rivers and is fed by the minor drainage system between them. Accurate core examination revealed the presence of thin, repeated paleosol sequences (Amorosi *et al.*, 2014). Late Pleistocene paleosols were tracked continuously across the triangle-shaped interchannel zone between the Reno and Savena rivers (Fig. 2). Less developed and more discontinuous paleosols characterize the Holocene succession (Bruno *et al.*, 2013).

## Methods

Six cores (SPZ100, SPZ20, SDH1, ASS1, INCL1 and INCL2, Fig. 3) were recovered between May and August 2016, in the Two Towers area. The rotary wash drilling method allowed high percentages (99.6%) of recovery of fine-grained sediments. Borehole depths ranged between 12 m (INCL 2) and 100 m (SPZ100) m. Core diameter was 101 mm, with the exception of core ASS1, which was drilled inside the Garisenda Tower, with a diameter of 60 mm. Cores INCL1 and 2 were inclined, respectively, at 15° and 30° to the vertical plane to collect samples beneath the Asinelli Tower foundation. In situ core descriptions and facies analysis relied on lithology, color, consistency and accessory material (e.g. vegetal remains, carbonate concretions, manganese and iron oxides). In situ pocket-penetrometer tests were carried out on cores SPZ100, SPZ20 and SDH1.

The uppermost 20 m of cores SPZ100, SPZ20, SDH1 and ASS1 were subsampled for laboratory analyses. In particular, 52 samples were collected for grain size determinations.

The hydrometer method (ASTM D7928-17, 2017) was used for the fine-grained soil fraction (i.e. diameter < 0.075 mm) and the sieving procedure for the remaining part of the samples. To investigate the possible influence of pedogenic processes (accumulation of organic matter and secondary calcite) on grain size distribution, eight additional soil samples were tested using the laser diffraction method (LDM; Alen, 1981; Bittelli *et al.*, 2019), with the Analysette 22 NanoTec Laser Particle Sizer by Fritsch. Five of these samples, in the clay–fine silt range (0.19–18.61 µm, Table 1), were analyzed before and after pretreatment with hydrogen peroxide (10 % solution) to remove organic matter. For the other three samples, in the coarse silt–fine sand range (9.5–911.7 µm, Table 2), tests were carried out before and after pretreatment with hydrochloric acid (HCl, 10 % solution) to remove carbonates. The organic matter content was determined as loss of ignition (ASTM F1647-11, 2018 – method A) in a 405 °C muffle furnace on 103 samples. Ninety samples were analyzed

to measure the CaCO<sub>3</sub> content using a 'Dietrich-Fruhling' calcimeter. Four-teen bulk sediment samples (Table 3) were dated by accelerator mass spectrometry (AMS) at Laboratory of Ion Beam Physics (ETH, Zurich, Switzerland). To avoid contamination from drilling fluids, samples were collected fresh from the innermost part of the core and desiccated in a 40 °C oven. All samples were cleaned from contaminations through acid–alkali–acid pretreatment. The <sup>14</sup>C dates were calibrated with OxCal 4.3 (Bronk Ramsey and Lee, 2013), using the IntCal13 calibration curve (Reimer et al., 2013). No optically stimulated luminescence (OSL) dating was possible due to the absence of sand intervals.

Core data were correlated along a stratigraphic cross-section (see Fig. 3 for location). Three additional core descriptions (S1, S2 and S16) from older drilling campaigns were reinterpreted, following calibration with new cores, to minimize data spacing along the section. To assess the relative influence of climate change on soil development, a dataset composed of 81 radiocarbon-dated paleosols from cores drilled in distinct sectors of the Po Plain was analyzed and compared with indicators of global and local climate oscillations (e.g.  $\delta^{18}\text{O}$  curves from ice cores, pollen series from lacustrine successions).

## Results

### *Depositional facies associations*

With the exception of two thin stratigraphic intervals encountered in core SPZ100 at 94.2–94.8 and 95.9–97.0 m depths, which consist of well-rounded pebbles in an abundant clay matrix, silt and clay are the dominant grain size fractions along the six cores. Three facies associations were identified within this mud-dominated succession.

### *Facies description*

'Swamp' facies association (SW, Fig. 4) was observed between 87.2 and 91.1 m core depth (Fig. 5). It is composed of soft, gray (5Y 7/2) silty clay with abundant undecomposed organic material (e.g. wood fragments and plant debris). Reaction to HCl was weak. Carbonate concretions, and Fe and Mn oxides were not observed. 'Poorly drained floodplain' facies association (PDFP) is composed of soft, light gray (10Y 8/2, 5 G 7/2, 5GY 8/1) silty clay (Fig. 4) showing weak reaction to HCl. Isolated carbonate nodules were rarely observed. Fe and Mn oxides were not observed. This facies association is poorly represented in the cores (Fig. 5). Its thickness is  $\leq 2$  m. 'Well-drained floodplain' facies association (WDFP) is the most well represented in cores. It is composed of hardened clayey silt and silty clay. Thickness exceeded 40 m (Fig. 5). Colors varied from grayish yellow (5Y 8/4) to light brownish gray (5YR 6/1), with yellowish mottles given by Fe oxides. Carbonate concretions were abundant at discrete horizons in the form of nodules, coatings or filaments along root traces. Reaction to HCl was strong, even where concretions were not detectable through visual inspection. Nodules of Mn oxides, root traces and slickensides were observed. Olive-grey and dusky brown (5Y 3/2, 5YR 2/2) horizons (Fig. 4), up to 2.3 m

thick, showing weak or no reaction to HCl, were present rhythmically along the core (Fig. 5). They generally overlie carbonate-rich horizons. Carbonate concretions were rare in the dark horizons.

### *Facies interpretation*

The dominance of fine-grained material along the cores suggests deposition in low-energy environments. The preservation of undecomposed organic material and a lack of oxides in facies association 'SW' suggests deposition under persistent reducing conditions. Local ponds or swamps may account for the deposition of this lithofacies.

Given the absence of Fe and Mn oxides, facies association 'PDFP' is interpreted as being deposited in a poorly drained floodplain, where waterlogging conditions are present only occasionally. The rare occurrence of carbonate nodules may be related to fluctuations of the groundwater table close to the topographic surface.

Based on color, consistency and the abundance of carbonate concretions and Fe–Mn oxides, facies association 'WDFP' is interpreted as deposited in a well-drained floodplain. Carbonate-free, dark intervals are interpreted as 'A' horizons of weakly developed palaeosols (Inceptisols of Soil Survey Staff, 1999). The dark color results from the deposition and decomposition of organic material in the topsoil. The local accumulation of carbonate concretions is interpreted to reflect illuviation from the topsoil to the underlying 'Bk' horizon. Nodules, coatings or filaments along root traces denote incipient soil development (Gile et al., 1981; Machette, 1985) associated with periods of subaerial exposure, on the order of a few thousand years. This estimate is substantiated by radio-carbon dates from similar paleosol profiles observed in the Bologna area (Amorosi et al., 2014). The mobilization and transfer of carbonates, which require the presence of a vadose zone, indicate a low groundwater table under conditions of subaerial exposure. Stratigraphic intervals, where subtle evidence of weathering (e.g. oxidation, root traces, reaction to HCl) was observed, are interpreted as 'Bw' horizons. The superposition of several soil profiles indicates multiple episodes of pedogenesis, interrupted by the deposition of overbank muds related to major flooding events. This process, along with continuous subsidence, was responsible for the accumulation and preservation of a > 40-m-thick 'WDFP' succession.

### *Paleosol characteristics*

Individual paleosols are 2–5 m thick and exhibit A-Bk, A-Bw or A-Bk-Bw profiles. The results of laboratory analyses confirm and provide quantification of the outcomes of core facies analysis. Partitioning of carbonates and organic matter in distinct soil horizons was clearly observed (Figs 6 and 7). The amount of CaCO<sub>3</sub> is 4.4 % in 'A' horizons, 22 % in 'Bw' horizons and 30 % in 'Bk' horizons (median values in Fig. 8A). In 'Bk' horizons, maximum values exceed 60 % (Figs 6 and 8A). The amount of organic matter is generally low ( $\leq 5$  %), with lowest values ( $\leq 3$  %) in the 'Bk' and 'Bw' horizons (Fig. 8B).

The amount of clay (median values in Fig. 8C) decreases from 'A' (38 %) to 'Bw' (26 %) horizons. The

percentage of silt increases in the same direction, from 51 to 59 % (median values in Fig. 8D). Sand is < 25 % (Figs 6 and 7). LDM tests show a marked reduction of clay percentage after pretreatment with hydrogen peroxide (Table 1). In particular, a greater reduction in clay percentage corresponds to a greater initial organic-matter content (i.e. ASS1\_10.6). Lower percentages of fine sand and coarse silt were observed in the samples pretreated with HCl (Table 2). The greatest sand–silt reductions were found for samples with the highest initial carbonate content (i.e. SPZ100\_9.9 m); SPZ20\_18 m is an exception, as it has the highest carbonate percentage (32 %), but a low percentage of coarse silt–fine sand (17.1 %) and therefore a minor particle reduction (8.6 %) compared to SPZ100\_9.9 m (16.2 %).

Organic matter, CaCO<sub>3</sub> and grain size vary significantly within individual soil profiles. In contrast, no substantial changes were observed comparing 'A' horizons from distinct soil profiles. The same conclusion derives from the comparison of 'Bk' and 'Bw' horizons from distinct paleosols.

### *Late Pleistocene paleosol architecture*

Based on the stratigraphic correlation with nearby core P515 (Fig. 2B), cored sediments were assigned to the Middle and Late Pleistocene. The Middle–Late Pleistocene boundary (i.e. the base of MIS 5e deposits) was tentatively placed around 39 m depth, at the base of poorly drained floodplain deposits in core SPZ100 (Fig. 5). Below this boundary, pocket penetration (PP) values fluctuate around a mean value of 3.2 kg cm<sup>2</sup>. By contrast, mean PP values of 2.2 kg cm<sup>2</sup> were measured in the Late Pleistocene–Holocene succession.

The uppermost 20 m was radiocarbon-dated almost entirely to the last 42 ka and four paleosols (P1, P2, P3 and PH, Fig. 9) were identified and correlated. As paleosol horizons at distinct stratigraphic levels can have similar physical properties and sedimentological characteristics, correlations were based on numerical ages and on the stratigraphic position of paleosols, rather than on their characteristics. Consistent with the chronological framework reported by Amorosi et al. (2014), paleosols P1, P2 and P3 were dated to MIS 3 and 2 (between ~42 and 23 cal ka BP, Table 3), whereas PH marks approximately the Late Pleistocene/Holocene transition (13–12 cal ka BP).

From base to top, paleosol characteristics can be summarized as follows:

1. Paleosol P1, 400–500 cm thick, has an A-Bk profile. The 'A' horizon is 65–155 cm thick.
2. Paleosol P2, 180–260 cm thick, has A-Bk or A-Bw profiles. The 'A' horizon is 75–140 cm thick.
3. Paleosol P3, 400–500 cm thick, has an A-Bk-Bw profile. Thickness of the 'A' horizon ranges between 85 and 230 cm. The 'Bk' horizon is relatively thin (<90 cm), whereas the 'Bw' horizon is up to 250 cm thick.
4. Paleosol PH, 240–380 cm thick, has A-Bk and locally A-Bk-Bw profiles. The 'A' horizon is ~80 cm thick. The 'Bk' horizon, 140–265 cm thick, has relatively high CaCO<sub>3</sub> content (37.8 %).

Minimum elevations of paleosols P2, P3 and PH were observed beneath the Garisenda tower (P1 was not encountered due to insufficient depth of ASS1). Paleosol P3 has lower elevation also beneath the Asinelli

tower, as observed in cores INCL1 and 2 (Fig. 9).

The Holocene succession is poorly preserved beneath the Two Towers, having been largely removed for the construction of the foundation structures. Holocene paleosols were observed in just two cores (Fig. 9). In SPZ100, two poorly developed paleosols (Entisols, Soil Survey Staff, 1999), 50–60 cm thick, overlie paleosol PH. In SDH1, a paleosol dated to 7.4 ka BP was found to be amalgamated with the underlying PH paleosol.

## Discussion

Soil development and burial in the Po Plain Consistent with the small drainage areas and poor transport capacity of creeks that supply sediment to the Bologna region, silt and clays are the dominant grain size fractions of the Middle and Late Pleistocene succession, down to 100m depth. Coarse - grained sediment (sand and gravel) is highly subordinate, as the Reno and Savena rivers never spread through this area during this period. Within this seemingly homogeneous floodplain succession, major textural and sedimentological changes are marked by buried soil horizons, which developed during time intervals shorter than 5000 years (Fig. 10). Between two successive phases of subaerial exposure, fluvial sedimentation led to deposition of relatively thin ( $\leq 5$ m) sediment packages that were entirely modified by pedogenic processes. Indeed, unweathered deposits ('C' or 'R' horizons) were not observed. The sharp increase in carbonate percentage at the transition from 'A' to underlying 'Bk' horizons (Figs. 6, 7 and 8A) suggests substantial vertical transfer of  $\text{CaCO}_3$  during pedogenesis. Relatively high carbonate contents in 'Bw' horizons (Fig. 8A), where carbonate concretions were not observed, suggest possible  $\text{CaCO}_3$  illuviation that also affected 'Bw' horizons. However, lacking micromorphological analyses, which would allow unequivocal distinction between primary and secondary calcite, it is difficult to estimate the amount of carbonates supplied by the parent rock material. The percentage of  $\text{CaCO}_3$  measured in the 'A' horizons (up to 15.7 %, Fig. 8A) may indicate either incomplete eluviation during subaerial exposure, or partial illuviation after burial, during the subsequent phase of soil formation. Higher percentages of silt and sand within 'B' horizons (Figs 6, 7 and 8D) may be partly due to the accumulation of secondary calcite in the form of micron- and millimeter-sized nodules or subtle coatings around clay particles. This hypothesis was confirmed by LDM tests carried out on samples pretreated with HCl, where a fine sand–coarse silt reduction was observed (Table 2).

While highly soluble compounds, such as  $\text{CaCO}_3$ , appear to be clearly involved in eluviation/illuviation processes, there is no evidence of clay mobilization and transfer along soil profiles, which is consistent with the relatively short period of subaerial exposure (Retallack, 2001; Buol et al., 2011). The clay content is highest in the 'A' horizons (Figs 6, 7 and 8C), probably due to the continuous mineralization of organic matter and its association with clay minerals (Kalisz et al., 2010; Yandong et al., 2018). This hypothesis was confirmed by the reduction of clay percentage after removal of organic matter with hydrogen peroxide. As a whole, vertical changes in grain size appear to be mainly controlled by pedogenesis rather than by sedimentary processes.

The relatively low amount of organic matter measured in the 'A' horizons (Figs 6, 7 and 8B) suggests low



groundwater levels during phases of subaerial exposure, which would have favored the rapid degradation of plant debris. Organic matter content in soil depends on the balance between the rates of addition and decomposition of organic material (Blair et al., 1995). It has been demonstrated that organic soils (organic carbon content of ~30 %) subjected to human-induced drainage (i.e. lowering of the water table) are affected by rapid and intense processes of organic matter transformation (e.g. mineralization, humification, changes in composition, and oxidation to CO<sub>2</sub>; Okruszko, 1993; Ilnicki and Zeitz, 2003; Okruszko and Ilnicki, 2003) that may lead to a drop in organic carbon content to ~5 % (Kalisz et al., 2010).

### *Climate control on soil development*

To assess whether paleosol development and burial at the Po Basin margin reflect a local or regional control, calendar ages on paleosols from the Bologna area were matched against radiocarbon dates from the central and distal parts of the Po Basin, far from the direct influence of Alpine glaciers (Fig. 10). It is noteworthy that numerical ages from paleosols P1, P2, P3 and PH are coincident across the entire region and invariably confined in the narrow range of 3.5–5 ka, with few local exceptions (see also Fig. 9). This implies that soil development occurred almost synchronously across distinct sectors of the Po Basin, thus suggesting predominantly external controlling factors.

Subsidence was a primary forcing factor at the scale of the entire Po River system, continuously creating accommodation for the accumulation of thick floodplain successions. The formation of paleosol P3 is linked to the rapid fall in sea level that occurred at the MIS 3–2 transition (~30–50 m between 30 and 24 cal ka BP, Peltier and Fairbanks, 2006). During this phase, the rate of sea level fall overcame subsidence rates and led to channel downcutting in the Po and Apenninic river systems. River incision prevented overbank flooding of adjacent interfluvial areas, and induced lowering of local groundwater levels (Tebbens et al., 1999), with the consequent development of paleosol P3 (Amorosi et al., 2014, 2017a).

Eustasy cannot account for the formation of paleosols P1 and P2, which formed in a period characterized by low-amplitude sea-level oscillations (Chappell, 2002). Far from the influence of sea level, river behavior (i.e. aggradation vs degradation) is controlled by the balance between sediment supply and water discharge (Blum and Törnqvist, 2000), which in turn can be altered by rapid climate changes (Erkens et al., 2011). For example, changes in vegetation type and density can induce short-lived periods of river instability (Vandenberghe, 2003) and modify the trajectory of pedogenesis dynamics.

If 14C dates are plotted against the  $\delta^{18}\text{O}$  curve from the NGRIP ice core (Svensson et al., 2008), one may note that the development of paleosols P1, P2 and P3 was systematically interrupted during peak-cold phases, at the culmination of Bond cycles (Bond et al., 1993), corresponding to North Atlantic Heinrich events (H in Fig. 10). Several pollen curves from European and Mediterranean lakes indicate variations in the vegetation cover related to high-frequency climate oscillations during MIS 3 (Fletcher et al., 2010; Helmens, 2014). In the

pollen record from Lagaccione (Magri, 1999) and Lake Firmon (Pini et al., 2010; see Fig. 1 for location) cold phases related to Heinrich events are marked by: (i) the dramatic reduction of taxa typical of temperate forests (e.g. *Quercus*, *Tilia* and *Abies*); and (ii) a parallel increase in herbs and xerophytes (Fig. 10). The pollen curve of core P515 (Bologna area, Amorosi et al., 2001) also records fluctuations in the amount of arboreal vegetation cover during the Late Pleistocene. However, a lack of radiocarbon dates between 45 and 10 ka BP prevents unequivocal correlations with paleosols P1 to PH.

We argue that the generalized reduction of the arboreal vegetation cover triggered by cold peaks at the end of Bond cycles enhanced erosion in the drainage basins and sediment transfer to the alluvial plains. Increased sediment supply promoted the filling of fluvial incisions and favored overbank flows, resulting in the burial of formerly exposed interfluvies. The rapid transition to warmer climate conditions at the onset of a new Bond cycle and the return to a denser vegetation cover inverted trends in the sediment supply/discharge ratio, promoting renewed channel incision and soil development in the adjacent interfluvial areas. This scenario can be envisaged for all paleosols, including P3, which is tentatively related to the Bond cycle between H3 and H2 (Fig. 10). Two isolated data younger than H2 (Fig. 10) are probably due to local morphological factors (e.g. pre-existing topography or distance from an active channel). Enhanced erosion during MIS 3 has been reported from several terrestrial archives (van Huissteden et al., 2001; Marković et al., 2014; Obreht et al., 2017). However, in these sites, correlation with climate fluctuations at the scale of Bond events was not possible due to limited chronological resolution. The Last Glacial Maximum, between H2 and H1, was characterized by an intense fluvial activity that led to the deposition of widespread channel-belt gravel and sand bodies (Amorosi et al., 2014; Campo et al., 2016), with consequent poor preservation of floodplain deposits (Morelli et al., 2017). Therefore, paleosols between 20 and 15 ka BP are encountered only locally (Bruno et al., 2015). Paleosol PH started to develop during the Bølling warm event, soon after H1, as recorded in three sites in the central Po Plain (Fig. 10). However, radiocarbon dates suggest that generalized pedogenesis occurred in the Po Basin (and in the Bologna area) during the Allerød warm phase, around 13.5 cal ka BP (Fig. 10). Coeval fluvial incision and soil development has also been recorded in other European fluvial systems (Mol, 1997; van Balen et al., 2010; Janssens et al., 2012). It is noticeable that the Younger Dryas (YD) cold reversal did not lead to the burial of paleosol PH, although this period is characterized by an intense sediment flux in the Po Plain (Amorosi et al., 2017a) and elsewhere (Abdulah et al., 2004; Anderson et al., 2004). Paleosol PH is associated with narrow and deep fluvial incisions (Morelli et al., 2017), through which large parts of the sediment eroded from the Apennine and Alpine catchments bypassed the Po Plain, accumulating downstream into the Adriatic Sea (Maselli et al., 2011). The YD event was probably too short-lived to lead to complete valley filling, resulting in scarce or no overbank sedimentation. The burial of paleosol PH occurred diachronously in the coastal plain after 10 ka BP, when this exposure surface was progressively transgressed during the post-MWP1B sea-level rise (Bruno et al., 2017a). In the Bologna area, less continuous

and less developed Holocene paleosols reflect increased accumulation rates after 10 ka BP (Bruno et al., 2017b). A buried soil, identified within eolian sediments ('Usselo layer'; Hošek et al., 2017a), has been dated to the Allerød interstadial in several sites in northern Europe, with sparse dates around the YD and the early Holocene (Kaiser et al., 2009). Although the 'Usselo' layer and paleosol PH formed in distinct geographical, sedimentary and ecological settings (and therefore they show peculiar textural and geochemical characteristics) the contemporary onset of pedogenesis in Italy and in northern Europe may have been driven by climate changes in the high-latitude Northern Hemisphere. Paleosol sequences from the subsiding Po Basin record variations in climate-related alluvial dynamics across MIS 3 and 2, with an unprecedented level of temporal resolution. Comparable records derive from the Eurasian loess–paleosol sequences, which bear evidence of past fluctuations in dust accumulation related to climate-driven changes in vegetation and pedogenesis (Chen et al., 1997; Haesaerts et al., 2016; Moine et al., 2017). However, with a few exceptions (Schirmer, 2016; Hošek et al., 2017b), the MIS 3 paleosol record of the European loess sequences is often incomplete. In alluvial settings, the formation of a paleosol has been linked to climate oscillations at a coarser scale (e.g. 21-ka precessional cycles, Abels et al., 2013). In general, MIS 3 deposits are poorly preserved in tectonically stable alluvial systems, due to widespread fluvial incision during the Late Pleistocene sea-level fall (Blum et al., 2013, and references therein). In the light of these remarks, the Po Basin paleosol sequence represents one of the best-preserved records of climate and environmental changes across MIS 3 and 2.

## Conclusions

A suite of vertically stacked, weakly developed paleosols beneath the 'Two Towers' of Bologna testifies to cyclical changes in alluvial dynamics during the Mid- to Late Pleistocene. Overbank deposition alternated with periods of subaerial exposure and soil development, shorter than 5000 years. Paleosols formed in a well-drained floodplain environment, where presumably low groundwater levels led to: (i) carbonate mobilization and transfer along the soil profile and (ii) intense degradation and oxidation of organic material.

The lack of evidence of clay mobilization is consistent with the relatively short exposure period.

Based on a vast chronological dataset, we document that the development and burial of paleosols occurred synchronously in the Bologna area and in other sectors of the Po Plain. Paleosol formation is inferred to reflect a combination of climatic and eustatic factors. Rhythmical climatic oscillations at the scale of the Bond cycles probably controlled paleosol development and burial during MIS 3. In particular, a dense arboreal vegetation during the warm part of each cycle favored soil development, whereas a more open vegetation cover at peak-cold termination of cycles led to drainage basin erosion, high sediment supply/discharge ratios and paleosol burial. An additional contribution from sea-level fall, which led to rapid channel downcutting, is called into question to explain soil formation at the MIS 3/2 transition. Eustatic rise was responsible for soil burial after 10 ka BP.

In alluvial settings, where sedimentary facies form typically lens-shaped sediment bodies, paleosols represent laterally extensive stratigraphic horizons that can record variations in sedimentary dynamics related to extrinsic factors. Weakly developed paleosols have been long neglected by stratigraphers, being considered less correlable than mature paleosols. This study demonstrates that Inceptisols are stratigraphic markers that can be traced on a basin scale. Compared to mature paleosols, which are associated with depositional hiatuses of tens of thousand years, repetitive sequences of weakly developed paleosols store a less fragmented record of past high-frequency (millennial-scale) climate fluctuations.

## **Data availability**

The data that support the findings of this study are available from the corresponding author upon reasonable request.

## **Acknowledgements.**

We acknowledge the Bologna municipality who funded the drilling campaign and provided access to the Two Towers historical site. This paper has been improved by the constructive suggestions of B. Giaccio and an anonymous reviewer.

## **Abbreviations.**

LDM, laser diffraction method; MIS, Marine Isotope Stage; OSL, optically stimulated luminescence; PP, pocket penetration; YD, Younger Dryas.

## **References**

Abdulah KC, Anderson JB, Snow JN et al. 2004. The late Quaternary Brazos and Colorado deltas, offshore Texas: their evolution and the factors that controlled their deposition. In Late Quaternary Stratigraphic Evolution of the Northern Gulf of Mexico Margin, Anderson JB, Fillon RH (eds). Society for Sedimentary Geology Special Publication, 237–269.

Abels HA, Kraus MJ, Gingerich PD. 2013. Precession-scale cyclicity in the fluvial Lower Eocene Willwood Formation of the Bighorn Basin, Wyoming (USA). *Sedimentology* 60: 1467–1483.

Allen T. 1981. Particle Size Analysis. Chapman & Hall: London.

Amorosi A, Bruno L, Campo B et al. 2017b. Global sea-level control on local parasequence architecture from

Amorosi A, Bruno L, Cleveland DM et al. 2017a. Paleosols and associated channel-belt sand bodies from a continuously subsiding late Quaternary system (Po Basin, Italy): new insights into continental sequence stratigraphy. *Geological Society of America Bulletin* 129: 449–463.

Amorosi A, Bruno L, Facciorusso J et al. 2016. Stratigraphic control on earthquake-induced liquefaction: A case study from the Central Po Plain (Italy). *Sedimentary Geology* 345: 42–53.

Amorosi A, Bruno L, Rossi V et al. 2014. Paleosol architecture of a late Quaternary basin–margin sequence and its implications for high- resolution, non-marine sequence stratigraphy. *Global and Planetary Change* 112: 12–25.

Amorosi A, Forlani L, Fusco F et al. 2001. Cyclic patterns of facies and pollen associations from Late Quaternary deposits in the subsurface of Bologna. *Geologica Acta* 1: 83–94.

Anderson JB, Rodriguez A, Abdulah KC et al. 2004. Late Quaternary stratigraphic evolution of the northern Gulf of Mexico margin: A synthesis. In *Late Quaternary Stratigraphic Evolution of the Northern Gulf of Mexico Margin*. In Society for Sedimentary Geology Special Publication, Anderson JB, Fillon RH (eds), 1–23.

Argnani A, Barbacini G, Bernini M et al. 2003. Gravity tectonics driven by Quaternary uplift in the Northern Apennines: insights from the La Spezia-Reggio Emilia geo-transect. In *Uplift and Erosion; Driving Processes and Resulting Landforms; Dynamic Relations Between Crustal and Surficial Processes*, Bartolini C, Piccini L, Catto NR (eds). *Quaternary International*, 13–26.

ASTM D7928-17. 2017. Standard Test Methods for Particle-Size Distribution (Gradation) of Fine-Grained Soils Using the Sedimentation (Hydrometer) Analysis. ASTM International: West Conshohocken.

ASTM. F1647-11. 2018. Standard Test Methods for Organic Matter Content of Athletic Field Rootzone Mixed.

ASTM International: West Conshohocken.

Bittelli M, Andrenelli MC, Simonetti G et al. 2019. Shall we abandon sedimentation methods for particle size analysis in soils? *Soil and Tillage Research* 185: 36–46.

Blair GJ, Lefroy R, Lisle L. 1995. Soil carbon fractions based on their degree of oxidation, and the development of a carbon management index for agricultural systems. *Australian Journal of Agricultural Research* 46: 1459–1466.

Blum MD, Martin J, Milliken K et al. 2013. Paleovalley systems: insights from Quaternary analogs and experiments. *Earth-Science Reviews* 116: 128–169.

Blum MD, Törnqvist TE. 2000. Fluvial responses to climate and sea-level change: a review and look forward. *Sedimentology* 47: 2–48. Bond G, Broecker W, Johnsen S et al. 1993. Correlations between climate records from North Atlantic sediments and Greenland ice. *Nature* 365: 143–147.

Bronk Ramsey C, Lee S. 2013. Recent and planned developments of the program OxCal. *Radiocarbon* 55(2-3): 720–730.

Bruno L, Amorosi A, Curina R et al. 2013. Human-landscape interactions in the Bologna area (Northern Italy) during the middle–late Holocene with focus on the Roman period. *Holocene* 23: 1558–1569.

Bruno L, Amorosi A, Severi P et al. 2015. High-frequency depositional cycles within the late Quaternary alluvial succession of Reno River (northern Italy). *Italian Journal of Geosciences* 134: 339–354.

Bruno L, Amorosi A, Severi P et al. 2017b. Late Quaternary aggradation rates and stratigraphic architecture of the southern Po Plain, Italy. *Basin Research* 29: 234–248.

Bruno L, Bohacs KM, Campo B et al. 2017a. Early Holocene transgressive palaeogeography in the Po coastal plain (northern Italy). *Sedimentology* 64: 1792–1816.

Buol SW, Southard RJ, Graham RC et al. 2011. *Soil Genesis and Classification*. Wiley-Blackwell: Chichester.

Cacciari M, Cremonini S, Marchesini M et al. 2017. When a pedomarker is lacking: palynological and chemical multianalysis of a Lateglacial-Holocene buried soils suite (Bologna, Italy). *International Journal of Environmental Quality* 24: 47–73.

Campo B, Amorosi A, Bruno L. 2016. Contrasting alluvial architecture of Late Pleistocene and Holocene deposits along a 120-km transect from the central Po Plain (northern Italy). *Sedimentary Geology* 341:

Carminati E, Di Donato G. 1999. Separating natural and anthropogenic vertical movements in fast subsiding areas: the Po Plain (N. Italy) case. *Geophysical Research Letters* 26: 2291–2294.

Carminati E, Doglioni C. 2012. Alps vs. Apennines: the paradigm of a tectonically asymmetric Earth. *Earth-Science Reviews* 112: 67–96.

Chappell J. 2002. Sea level changes forced ice breakouts in the last glacial cycle: new results from coral terraces. *Quaternary Science Reviews* 21: 1229–1240.

Chen FH, Bloemendal J, Wang JM et al. 1997. High-resolution multi-proxy climate records from Chinese loess: evidence for rapid climatic changes over the last 75 kyr. *Palaeogeography, Palaeoclimatology, Palaeoecology* 130: 323–335.

Choi K. 2005. Pedogenesis of late Quaternary deposits, northern Kyonggi bay, Korea: implications for relative sea-level change and regional stratigraphic correlation. *Palaeogeography, Palaeoclimatology, Palaeoecology* 220: 387–404.

Cleveland DM, Atchley SC, Nordt LC. 2007. Continental Sequence Stratigraphy of the Upper Triassic (Norian Rhaetian) Chinle Strata, Northern New Mexico, U.S.A.: Allocyclic and Autocyclic Origins of Paleosol-Bearing Alluvial Successions. *Journal of Sedimentary Research* 77: 909–924.

Demko TM, Currie BS, Nicoll KA. 2004. Regional paleoclimatic and stratigraphic implications of paleosols and fluvial/overbank architecture in the Morrison Formation (Upper Jurassic), Western Interior, USA. *Sedimentary Geology* 167: 115–135.

Doglioni C, Gueguen E, Harabaglia P et al. 1999. On the origin of west-directed subduction zones and applications to the western Mediterranean. In *The Mediterranean Basins; Tertiary Extension Within the Alpine Orogen*, Durand B, Jolivet L, Horváth F et al. (eds). Geological Society Special Publications, 541–561.

Dubiel RF, Hasiotis ST. 2011. Deposystems, paleosols, and climatic variability in a continental system: the Upper Triassic Chinle Formation, Colorado Plateau, U.S.A. In *From River to Rock Record: the Preservation of Fluvial Sediments and Their Subsequent Interpretation*, Davidson SK, Leleu S, North CP (eds). Society for

Erkens G, Hoffmann T, Gerlach R et al. 2011. Complex fluvial response to Lateglacial and Holocene allogenic forcing in the Lower Rhine Valley (Germany). *Quaternary Science Reviews* 30: 611–627.

Fletcher WJ, Sánchez Goñi MF, Allen JRM et al. 2010. Millennial-scale variability during the last glacial in vegetation records from Europe. *Quaternary Science Reviews* 29: 2839–2864.

Gile LH, Hawley JW, Grossman RB. 1981. *Soils and Geomorphology in the Basin and Range Area of Southern New Mexico – Guidebook to the Desert Project*. New Mexico Bureau of Mines and Mineral Resources: Socorro.

Haesaerts P, Damblon F, Gerasimenko N et al. 2016. The Late Pleistocene loess-palaeosol sequence of Middle Belgium. *Quaternary International* 411: 25–43.

Helmens KF. 2014. The Last Interglacial–Glacial cycle (MIS 5–2) re-examined based on long proxy records from central and northern Europe. *Quaternary Science Reviews* 86: 115–143.

Hošek J, Lisá L, Hambach U et al. 2017b. Middle Pleniglacial pedogenesis on the northwestern edge of the Carpathian basin: A multidisciplinary investigation of the Bíňa pedo-sedimentary section, SW Slovakia. *Palaeogeography, Palaeoclimatology, Palaeoecology* 487: 321–339.

Hošek J, Pokorný P, Prach J et al. 2017a. Late Glacial erosion and pedogenesis dynamics: evidence from high-resolution lacustrine archives and paleosols in south Bohemia (Czech Republic). *CATENA* 150: 261–278.

Ilnicki P, Zeitz J. 2003. Irreversible loss of organic soil functions after reclamation. In *Organic Soils and Peat Materials for Sustainable Agriculture*, Parent LE, Ilnicki P (eds). CRC Press: Boca Raton; 15–32.

Janssens MM, Kasse C, Bohncke SJP et al. 2012. Climate-driven fluvial development and valley abandonment at the last glacial–interglacial transition (Oude IJssel-Rhine, Germany). *Netherlands Journal of Geosciences - Geologie en Mijnbouw* 91: 37–62.

Kaiser K, Hilgers A, Schlaak N et al. 2009. Palaeopedological marker horizons in northern central Europe: characteristics of Lateglacial Usselo and Finow soils. *Boreas* 38: 591–609.



Kalisz B, Lachacz A, Glazewski R. 2010. Transformation of some organic matter components in organic soils exposed to drainage. *Turkish Journal of Agriculture and Forestry* 34: 245–256.

Kraus MJ. 1999. Paleosols in clastic sedimentary rocks: their geologic applications. *Earth-Science Reviews* 47: 41–70.

Kraus MJ, Bown TM. 1993. Palaeosols and sandbody prediction in alluvial sequences. In *Characterization of Fluvial and Aeolian Reservoirs*, North CP, Prosser DJ (eds). Geological Society of London Special Publication, 23–31.

Yandong MA, Jingbo Z, Rui L et al. 2018. Formation and movement of groundwater in the thick loess-palaeosol sequences of the Chinese Loess Plateau. *Pedosphere* 28: 895–904.

Machette MN. 1985. Calcic soils of the southwestern United States. *Geological Society of America Special Papers* 203: 1–22.

Magri D. 1999. Late Quaternary vegetation history at Lagaccione near Lago di Bolsena (central Italy). *Review of Palaeobotany and Palynology* 106: 171–208.

Marković SB, Hambach U, Stevens T et al. 2012. Relating the astronomical timescale to the loess–paleosol sequences in Vojvodina, Northern Serbia. In *Climate Change: Inferences from Paleoclimate and Regional Aspects*, Berger A, Mesinger F, Sijacki D (eds). Springer-Verlag: Vienna; 65–78.

Marković SB, Timar-Gabor A, Stevens T et al. 2014. Environmental dynamics and luminescence chronology from the Orlovat loess–palaeosol sequence (Vojvodina, northern Serbia). *Journal of Quaternary Science* 29: 189–199.

Maselli V, Hutton EW, Kettner AJ et al. 2011. High-frequency sea level and sediment supply fluctuations during Termination I: An integrated sequence-stratigraphy and modeling approach from the Adriatic Sea (central Mediterranean). *Marine Geology* 287: 54–70.

McCarthy PJ, Plint AG. 2003. Spatial variability of palaeosols across Cretaceous interfluvies in the Dunvegan Formation, NE British Columbia, Canada: palaeohydrological, palaeogeomorphological and stratigraphic implications. *Sedimentology* 50: 1187–1220.

Moine O, Antoine P, Hatté C et al. 2017. The impact of Last Glacial climate variability in west-European loess revealed by radiocarbon dating of fossil earthworm granules. *Proceedings of the National Academy of Sciences of the United States of America* 114: 6209–6214. Mol J. 1997. Fluvial response to Weichselian climate changes in the Niederlausitz (Germany). *Journal of Quaternary Science* 12: 43–60.

Morelli A, Bruno L, Cleveland DM et al. 2017. Reconstructing Last Glacial Maximum and Younger Dryas paleolandscapes through subsurface paleosol stratigraphy: an example from the Po coastal plain, Italy. *Geomorphology* 295: 790–800.

Muttoni G, Carcano C, Garzanti E et al. 2003. Onset of major Pleistocene glaciations in the Alps. *Geology* 31: 989–992. <https://doi.org/10.1130/G19445.1>

Obrecht I, Hambach U, Veres D et al. 2017. Shift of large-scale atmospheric systems over Europe during late MIS 3 and implications for Modern Human dispersal. *Scientific Reports* 7: 5848.

Okrusko H. 1993. Transformation of fen-peat soils under the impact of draining. *Zesz Probl Post Nauk Roln* 406: 3–73.

Okrusko H, Ilnicki P. 2003. The moorsh horizons as quality indicators of reclaimed organic soils. In *Organic Soils and Peat Materials for Sustainable Agriculture*, Parent LE, Ilnicki P (eds). CRC Press: Boca Raton; 1–14.

Peltier WR, Fairbanks RG. 2006. Global glacial ice volume and Last Glacial Maximum duration from an extended Barbados sea level record. *Quaternary Science Reviews* 25: 3322–3337.

Pini R, Ravazzi C, Reimer PJ. 2010. The vegetation and climate history of the last glacial cycle in a new pollen record from Lake Fimon (southern Alpine foreland, N-Italy). *Quaternary Science Reviews* 29: 3115–3137.

Reimer PJ, Bard E, Bayliss A et al. 2013. IntCal13 and Marine13 radiocarbon age calibration curves 0–50,000 years cal BP. *Radio- carbon* 55: 1869–1887.

Retallack GJ. 2001. *Soils of the Past: an Introduction to Paleopedology*. Blackwell Publishing: Oxford.

Ricci Lucchi F. 1986. Oligocene to Recent foreland basins of Northern Apennines. In *Foreland Basins*, Allen P, Homewood P (eds). International Association of Sedimentologists, Special Publications, 105–139.

Schirmer W. 2016. Late Pleistocene loess of the Lower Rhine. *Quaternary International* 411: 44–61.

Sheldon ND, Tabor NJ. 2009. Quantitative paleoenvironmental and paleoclimatic reconstruction using paleosols. *Earth-Science Reviews* 95: 1–52.

Soil Survey Staff. 1999. *Soil Taxonomy. A basic system of soil classification for making and interpreting soil surveys*, Agricultural Handbook. no. 436. Natural Resources Conservation Service, USDA: Washington, DC.

Srivastava P, Sinha R, Deep V et al. 2018. Micromorphology and sequence stratigraphy of the interfluvial paleosols from the Ganga plains: a record of alluvial cyclicity and paleoclimate during the late Quaternary. *Journal of Sedimentary Research* 88: 105–128.

Svensson A, Andersen KK, Bigler M et al. 2008. A 60000 year Greenland stratigraphic ice core chronology. *Climate of the Past* 4: 47–57.

Tebbens LA, Veldkamp A, Westerhoff W et al. 1999. Fluvial incision and channel downcutting as a response to Late-glacial and Early Holocene climate change: the lower reach of the River Meuse (Maas), The Netherlands. *Journal of Quaternary Science* 14: 59–75.

Tsatskin A, Sandler A, Avnaim-Katav S. 2015. Quaternary subsurface paleosols in Haifa Bay, Israel: A new perspective on stratigraphic correlations in coastal settings. *Palaeogeography, Palaeoclimatology, Palaeoecology* 426: 285–296.

van Balen RT, Busschers FS, Tucker GE. 2010. Modeling the response of the Rhine–Meuse fluvial system to Late Pleistocene climate change. *Geomorphology* 114: 440–452.

van Huissteden J(ko), Gibbard PL, Briant RM. 2001. Periglacial fluvial systems in northwest Europe during marine isotope stages 4 and 3. *Quaternary International* 79: 75–88.

Vandenberghe J. 2003. Climate forcing of fluvial system development: an evolution of ideas. *Quaternary Science Reviews* 22: 2053–2060.

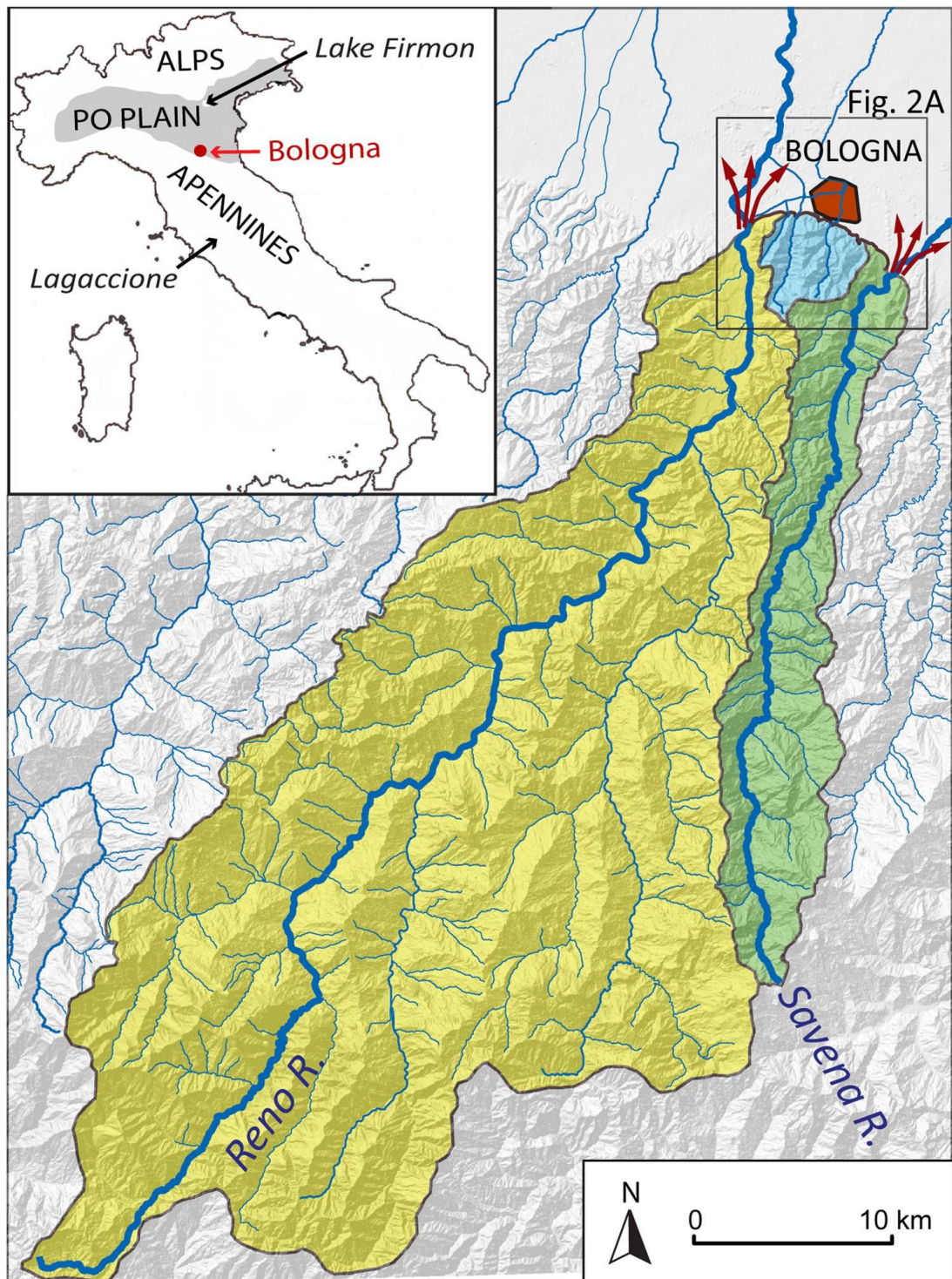


Figure 1. Drainage basins (and related alluvial fan systems) of the Reno (yellow) and Savena (green) Apennine rivers, compared with small creeks draining the much smaller area south of Bologna (light blue).



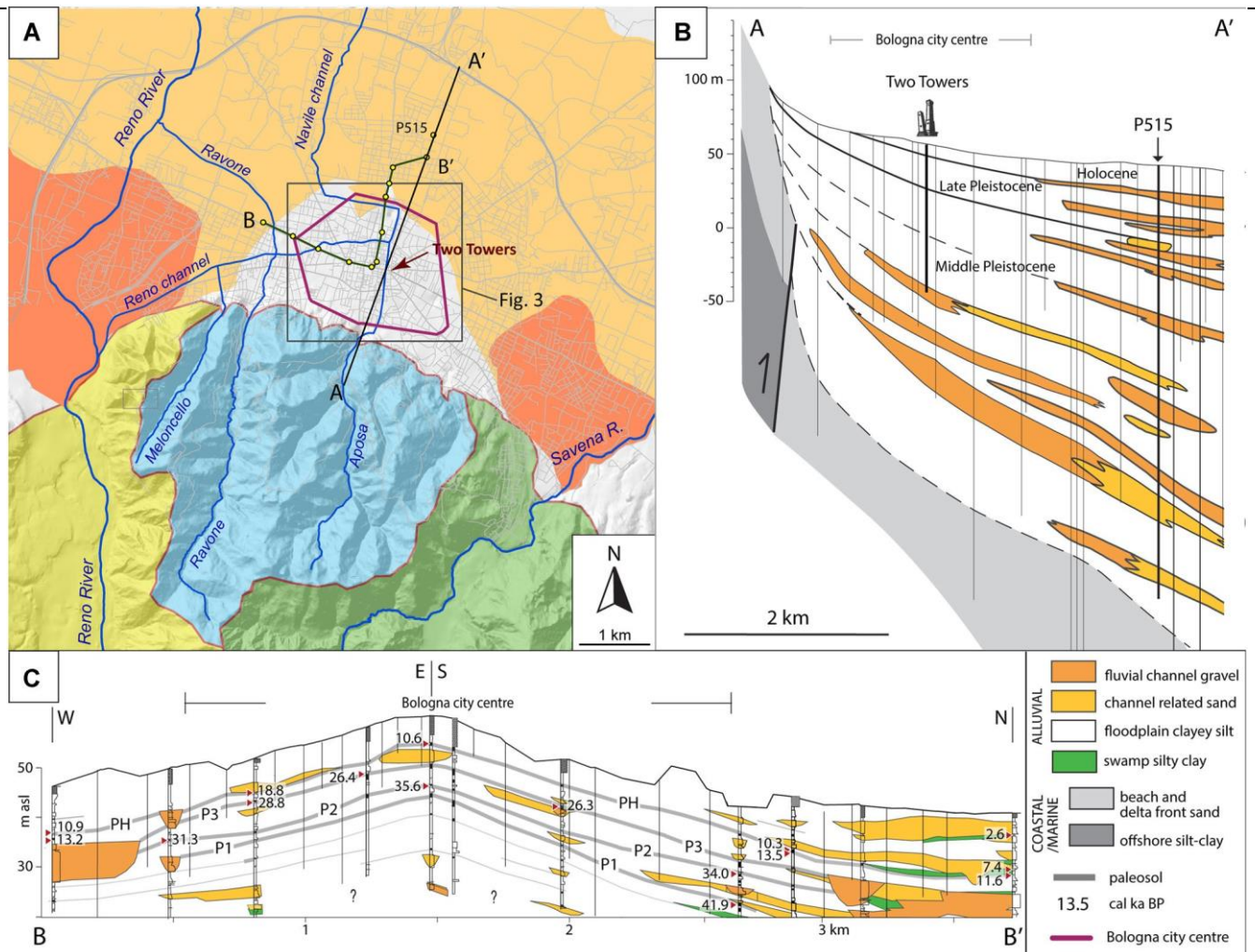


Figure 2. (A) Close up on the Bologna urban area and on its adjoining foothills. Amalgamated fluvial-channel gravel bodies form alluvial fan systems (red areas) close to the Reno and Savena outlets. Gravel-mud alternations are present at more distal locations (orange area). (B) Subsurface stratigraphy of the Bologna area along a stratigraphic panel transverse to the Apennine chain (modified after Amorosi et al., 2001). Note a lack of coarse-grained deposits in the uppermost 100 m beneath the historical center. (C) Stratigraphic profile across the historical center of Bologna, showing the high correlation potential of Late Pleistocene paleosols P1, P2, P3 and PH (modified after Amorosi et al., 2014).

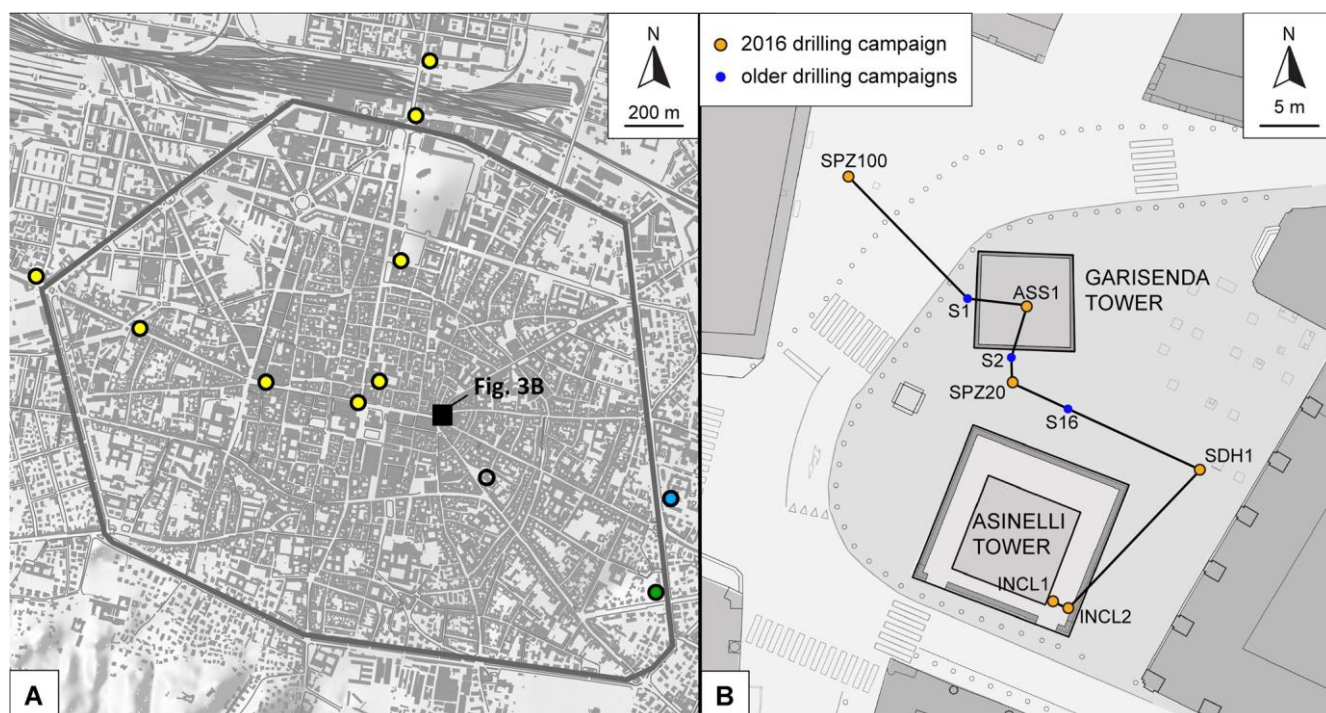


Figure 3. (A) The Medieval center of Bologna, with location of the study area and of additional radiocarbon-dated cores and outcrops used in this work. Yellow circles are cores from Amorosi et al. (2014); green and blue circles are outcrops described in the Geological Map of Italy at 1:50 000 scale (Sheet 221 - Bologna) and in Cacciari et al. (2017), respectively. The open circle marks a core from which a new radiocarbon date was obtained. (B) The 'Two Towers' study area, with location of the analyzed cores.

Table 1. Results of particle size distribution tests with the laser diffraction method (LDM): comparison between paleosol samples pretreated with hydrogen peroxide (used to remove organic matter) and non-pretreated samples.

	Organic matter content (%)	Clay percentage (%) (<0.002 mm)	Pretreated clay percentage (%) (<0.002 mm)
ASS1_11.6 m	2.50	26.6	25.8
ASS1_10.6 m	3.14	24.1	19.0
ASS1_7.75 m	1.80	30.4	29.9
SDH1_13 m	2.31	20.7	19.8
SPZ20_12 m	2.30	18.6	16.5

Table 2. Results of particle size distribution tests with the laser diffraction method (LDM): comparison between paleosol samples pretreated with hydrochloric acid (used to remove carbonates) and non-pretreated samples.

	Carbonate content (%)	Sand percentage (%) (>0.075 mm)	Pretreated sand percentage (%) (>0.075 mm)
SPZ100_9.9 m	28.5	46.0	29.8
SPZ20_10.1 m	22.0	18.9	11.9
SPZ20_18 m	32.0	17.1	8.5

Table 3. List of radiocarbon-dated paleosol samples of Fig. 3B and 9.

Core	Depth (m)	Code	$^{14}\text{C}$ age (BP)	$2\sigma$ calibrated age (BP, median $\pm$ error)
SPZ100	3.43	ETH-92213	$5820 \pm 26$	$6630 \pm 40$
SPZ100	4.7	ETH-92222	$10\,869 \pm 31$	$12\,740 \pm 20$
SPZ100	7.74	ETH-92219	$21\,332 \pm 88$	$25\,680 \pm 100$
ASS1	7.1	ETH-90589	$11\,175 \pm 40$	$13\,050 \pm 40$
ASS1	10.3	ETH-90593	$22\,343 \pm 67$	$26\,620 \pm 170$
ASS1	15.2	ETH-90591	$29\,452 \pm 111$	$33\,700 \pm 100$
SPZ20	4.8	ETH-90592	$6502 \pm 36$	$7410 \pm 45$
SPZ20	4.95	ETH-92217	$10\,448 \pm 30$	$12\,390 \pm 110$
SPZ20	7.9	ETH-98602	$20\,230 \pm 46$	$24\,300 \pm 100$
SPZ20	11,9	ETH-98603	$28\,844 \pm 305$	$32\,940 \pm 440$
SPZ20	15.2	ETH-90588	$37\,923 \pm 195$	$42\,200 \pm 160$
SDH1	8.5	ETH-90587	$19\,408 \pm 58$	$23\,350 \pm 130$
INCL1	9.4	ETH-90594	$22\,525 \pm 69$	$26\,850 \pm 160$
INCL2	10.8	ETH-90595	$21\,043 \pm 63$	$25\,400 \pm 110$

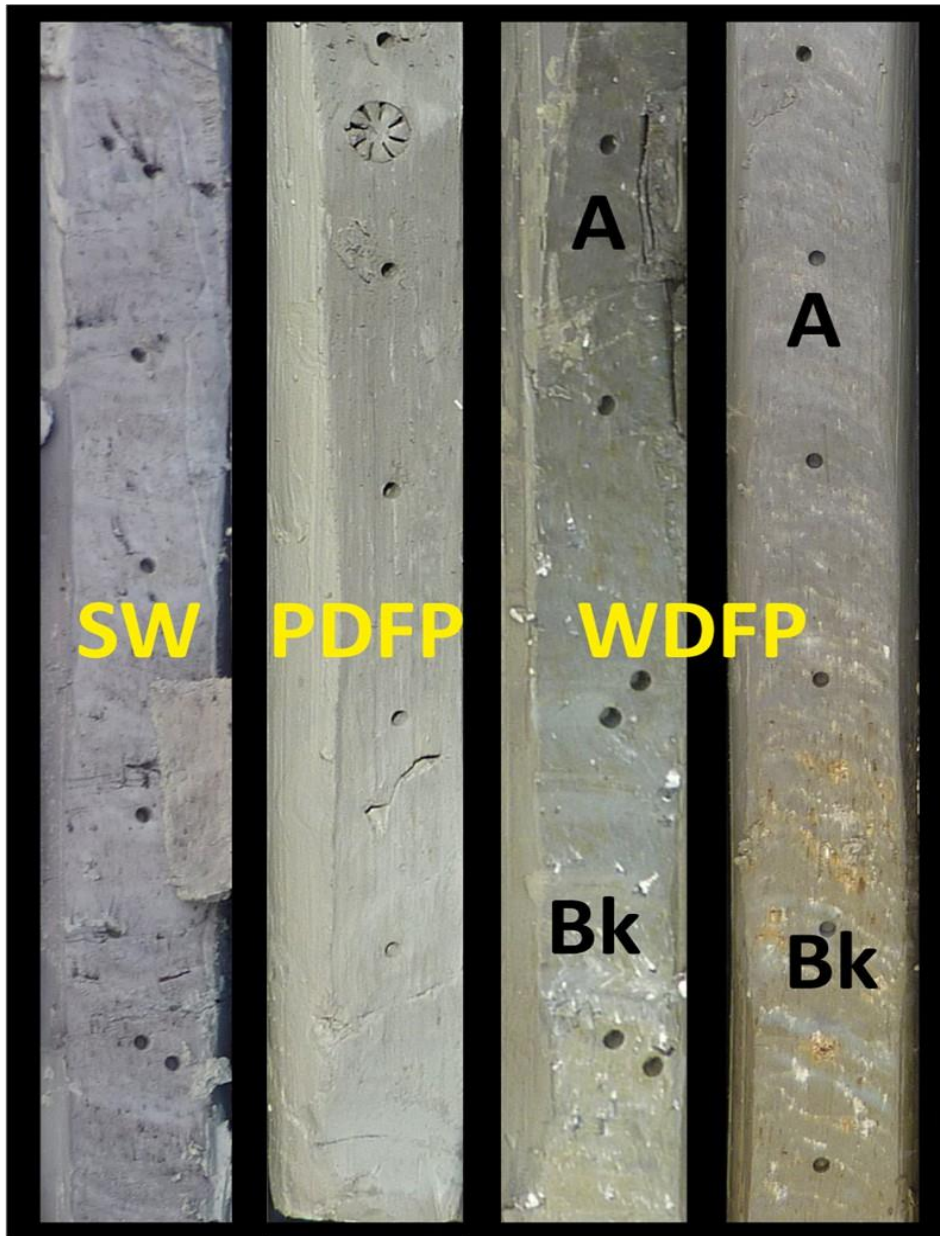
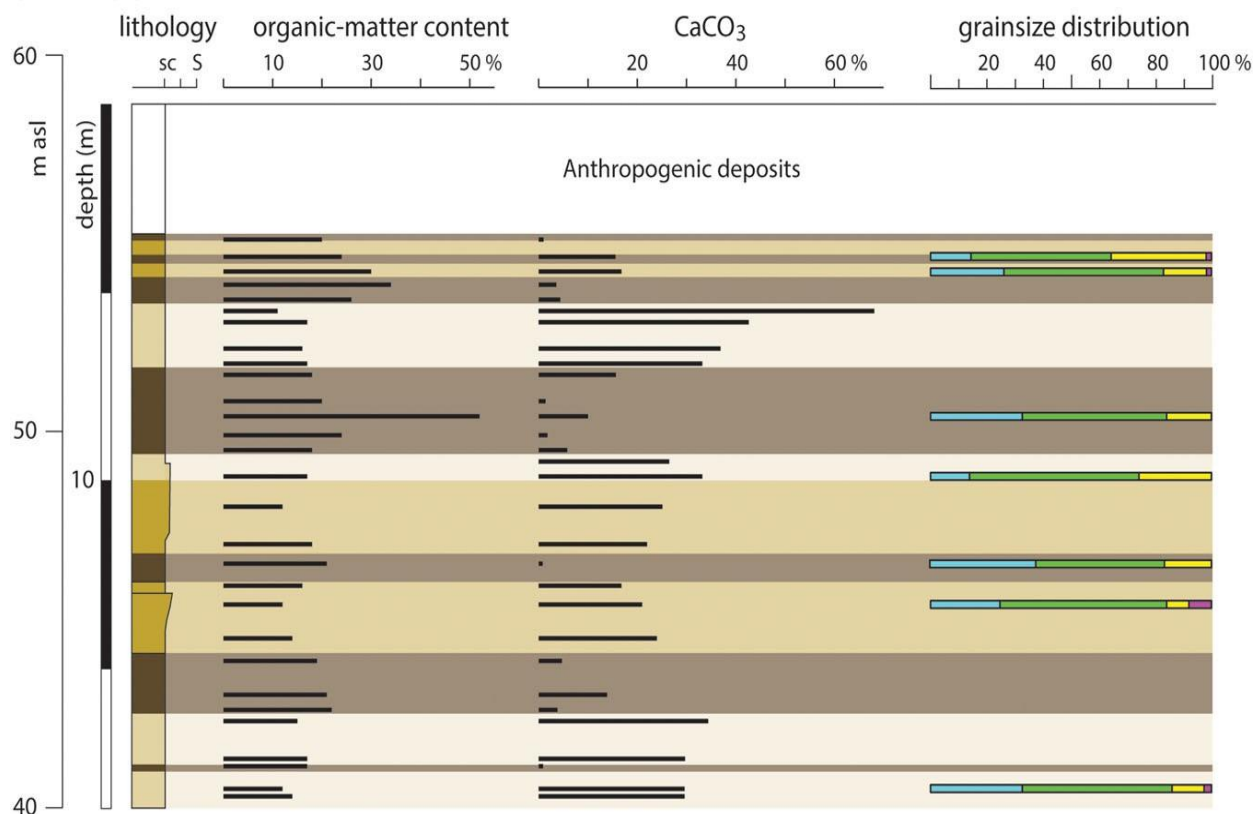


Figure 4. Representative photographs of the facies associations identified in core SPZ100. From left to right: SW, organic-matter-rich swamp clays; PDFP, poorly drained floodplain clayey silt and silty clay; WDFP, varicolored and hardened well-drained floodplain clayey silt. For detailed description of paleosol horizons 'A' and 'Bk', see text.

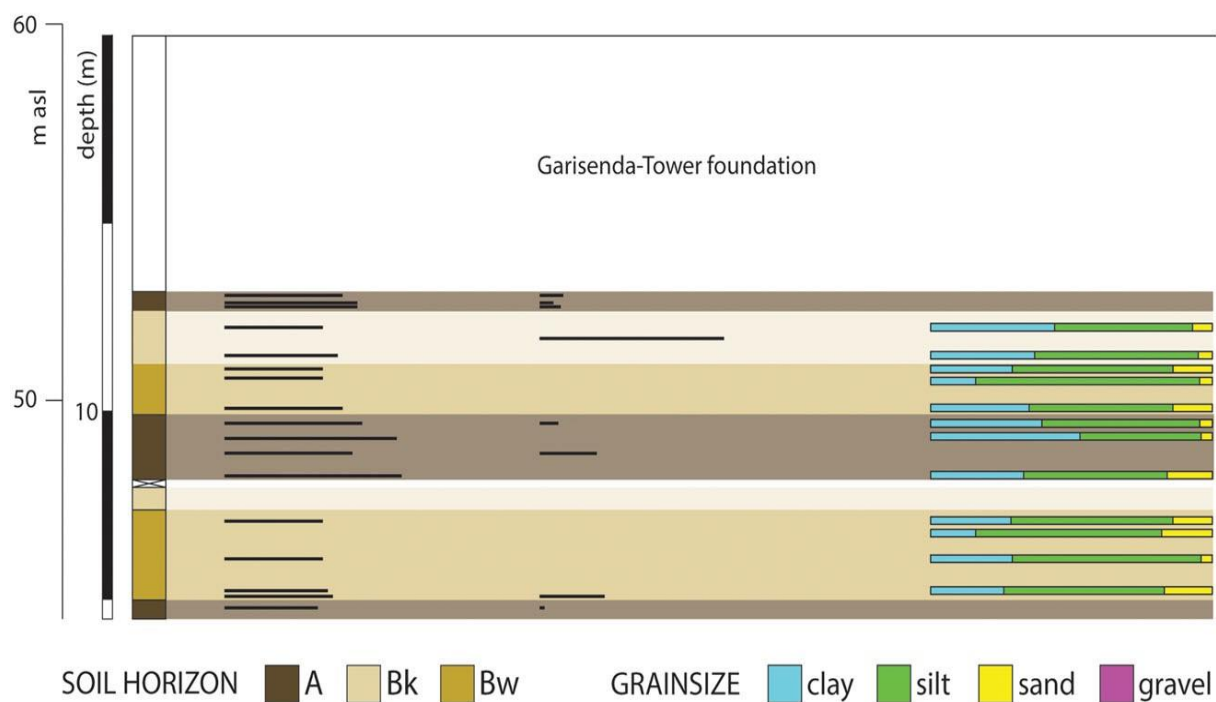




## SPZ 100



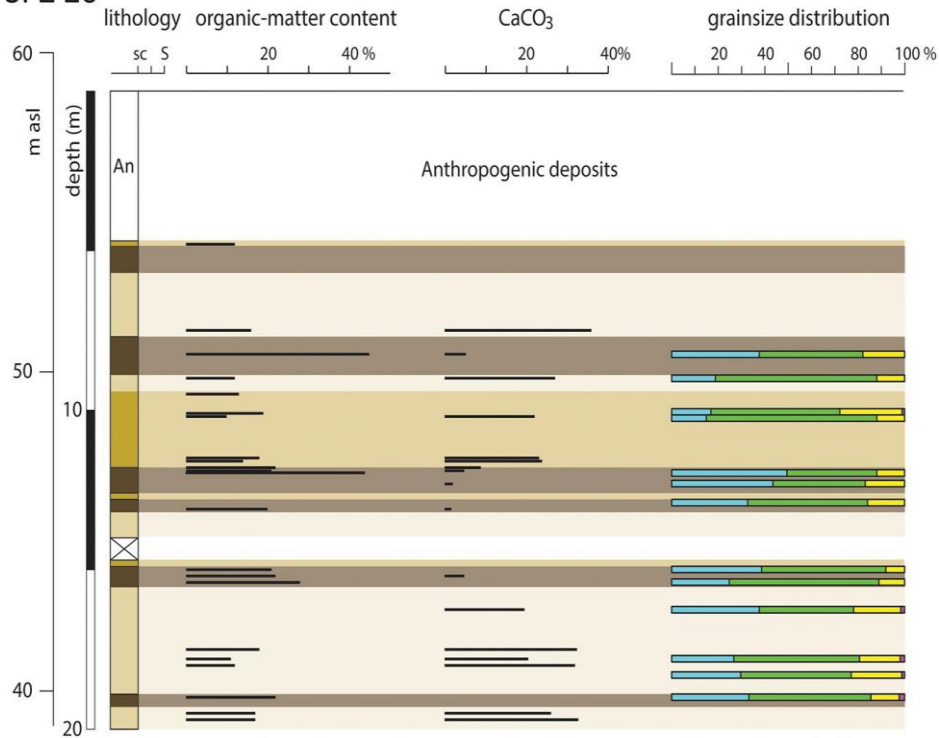
## ASS 1



SOIL HORIZON    A    Bk    Bw    GRAINSIZE    clay    silt    sand    gravel

Figure 6. Vertical distribution of organic matter,  $\text{CaCO}_3$  content and grain size along distinct paleosol horizons from cores SPZ100 and ASS1. See Fig. 3 for location.

## SPZ 20



## SDH1

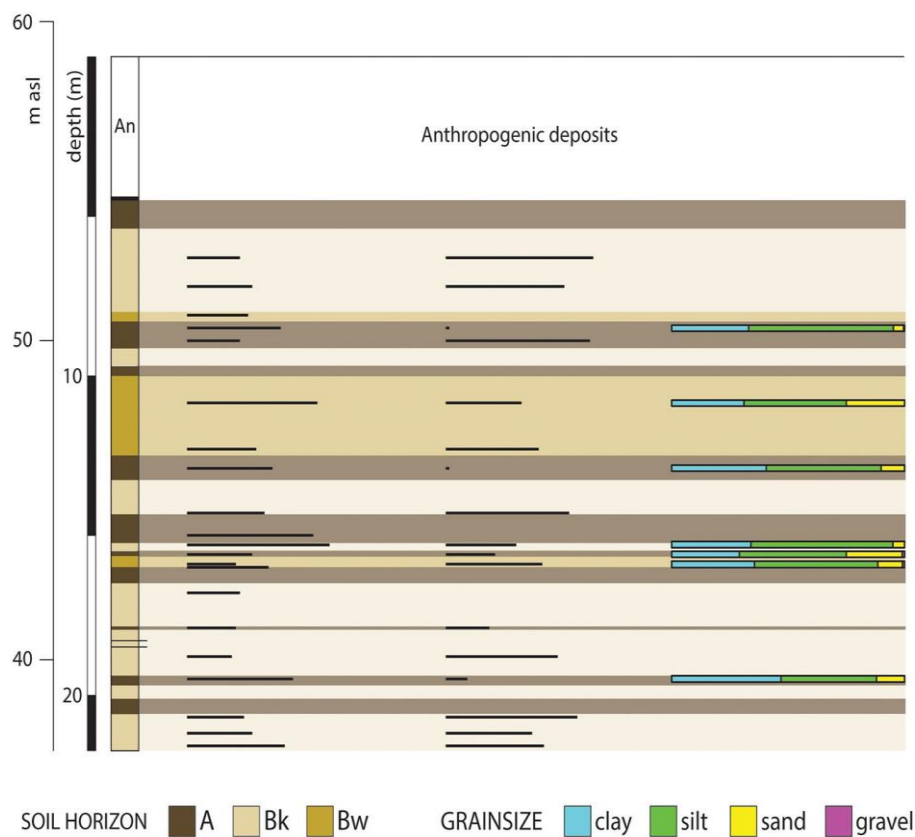


Figure 7. Vertical distribution of organic matter,  $\text{CaCO}_3$  content and grain size along distinct paleosol horizons from cores SPZ20 and SDH1. See Fig. 3 for location.

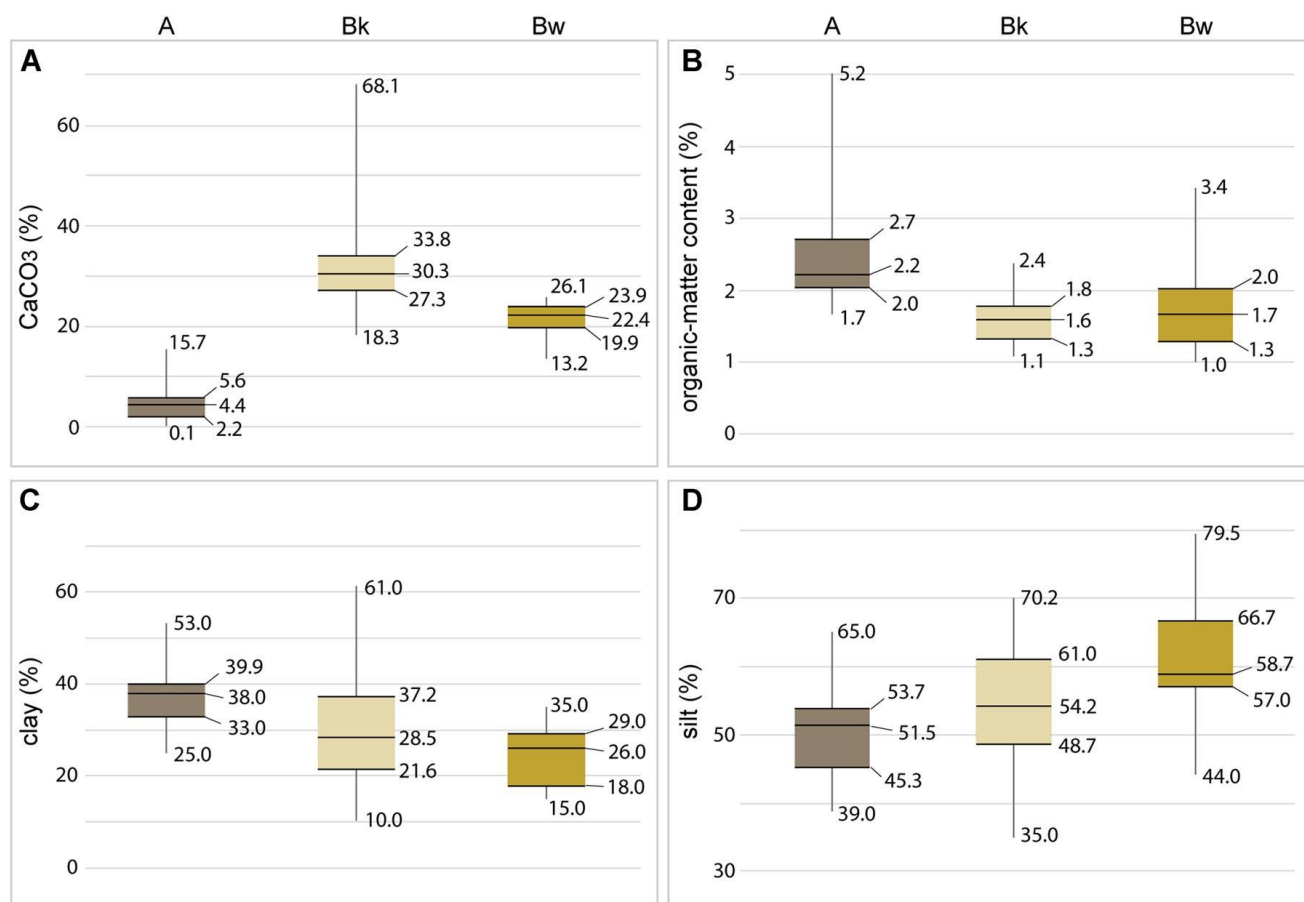


Figure 8. Boxplot graph showing percentages of CaCO<sub>3</sub> (A), organic matter (B), clay (C) and silt (D) in the 'A', 'Bk' and 'Bw' horizons of the analyzed paleosols. Minimum and maximum values (lower and upper limits of vertical bars, respectively), the first and the third quartiles (horizontal bars at the base and top of colored boxes, respectively) and median values (horizontal bars within the boxes) are represented. 'A' horizons are characterized by the lowest carbonate contents and the highest organic matter and clay contents. 'Bk' horizons exhibit the highest CaCO<sub>3</sub> contents. Less marked differences in organic matter, clay and silt content are observed between 'Bk' and 'Bw' horizons.

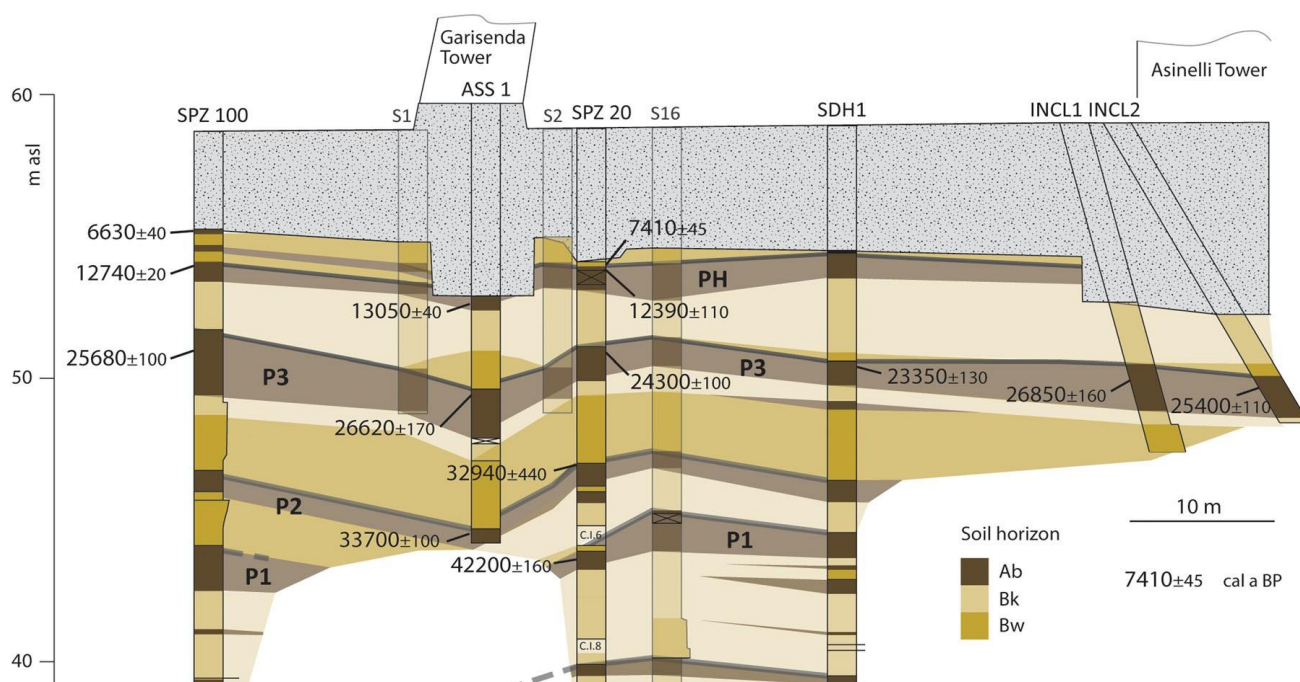


Figure 9. Stratigraphic correlation of Late Pleistocene paleosols P1, P2, P3 and PH across the study area. See Fig. 3B for core

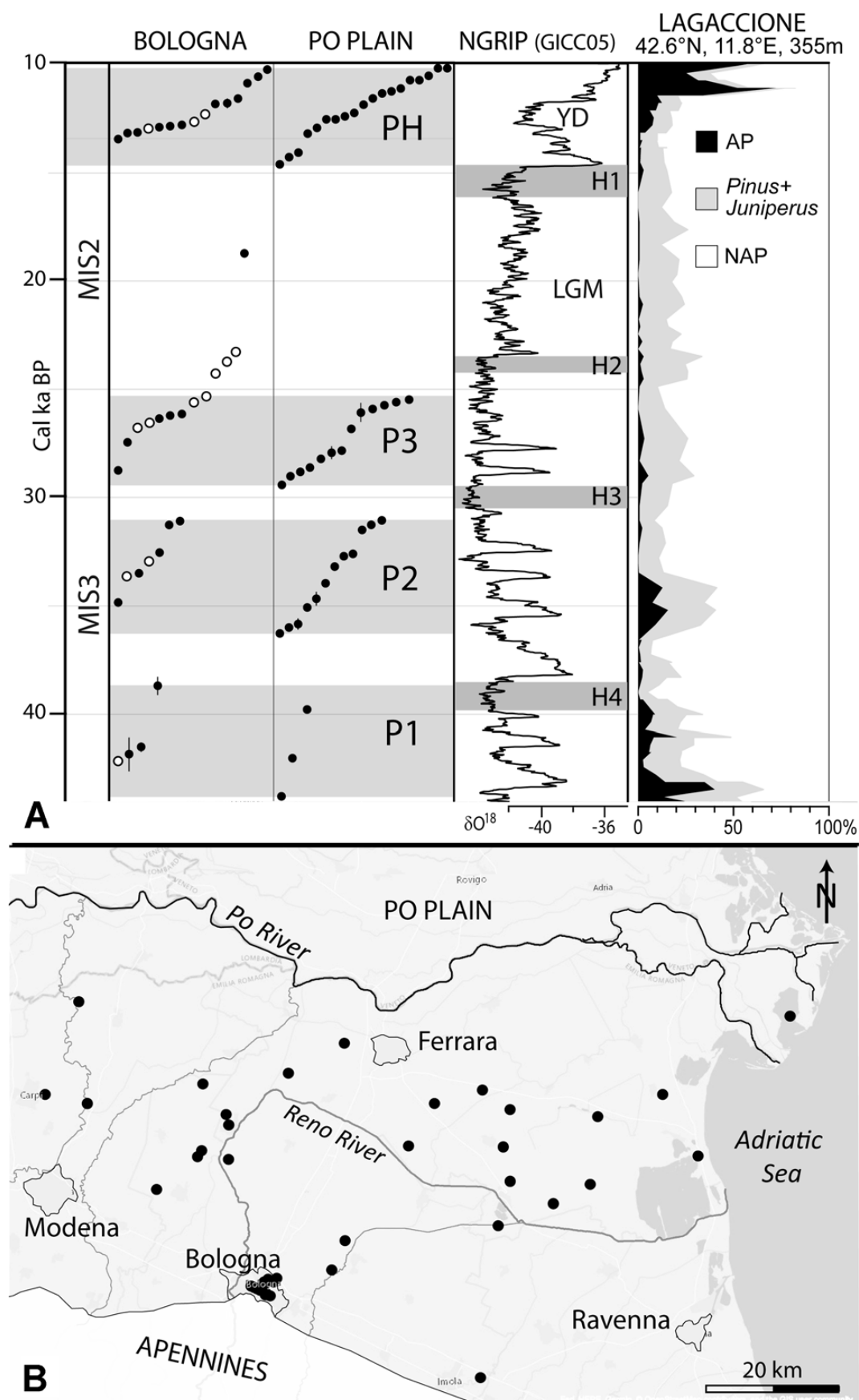


Figure 10. (A) Paleosol chronostratigraphy from the Bologna area and the Po Plain and its correlation with the  $\delta^{18}O$  curve from the NGRIP ice core (Svensson *et al.*, 2008) and the pollen record from Lagaccione (central Italy, modified after Fletcher *et al.*, 2010; location on Fig. 1). Radiocarbon dates on paleosols are from this work (open circles) or from published papers and maps (black circles; sheets 205, 221 and 222 of the Geological Map of Italy 1:50 000 scale, Amorosi *et al.*, 2014, 2016, 2017a,b; Cacciari *et al.*, 2017). AP, arboreal pollen; NAP, non-arboreal pollen. (B) Location of the radiocarbon- dated cores shown in A.